

Magnetoresistive system with concentric ferromagnetic asymmetric nanorings

J. I. Avila, M. A. Tumelero, A. A. Pasa, and A. D. C. Viegas

Citation: *Journal of Applied Physics* **117**, 103901 (2015); doi: 10.1063/1.4914346

View online: <http://dx.doi.org/10.1063/1.4914346>

View Table of Contents: <http://scitation.aip.org/content/aip/journal/jap/117/10?ver=pdfcov>

Published by the [AIP Publishing](#)

Articles you may be interested in

[Controlling vortex chirality and polarity by geometry in magnetic nanodots](#)

Appl. Phys. Lett. **104**, 012407 (2014); 10.1063/1.4861423

[Domain wall induced magnetoresistance in a superconductor/ferromagnet nanowire](#)

Appl. Phys. Lett. **99**, 032501 (2011); 10.1063/1.3610947

[Magnetic imaging of the pinning mechanism of asymmetric transverse domain walls in ferromagnetic nanowires](#)

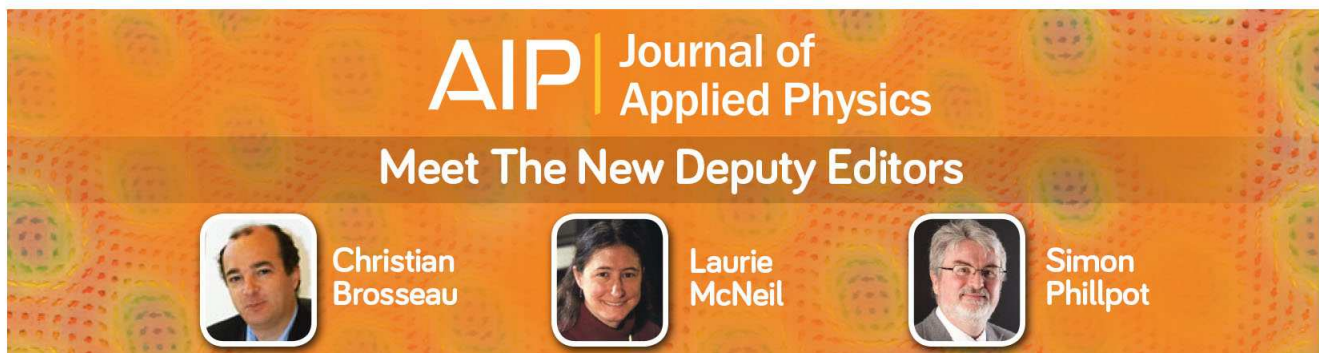
Appl. Phys. Lett. **97**, 233102 (2010); 10.1063/1.3523351

[Asymmetric ground state spin configuration of transverse domain wall on symmetrically notched ferromagnetic nanowires](#)

Appl. Phys. Lett. **97**, 022511 (2010); 10.1063/1.3459965

[Dispersion of the pinning field direction of a ferromagnet/antiferromagnet coupled system](#)

Appl. Phys. Lett. **78**, 237 (2001); 10.1063/1.1335842

A promotional banner for the Journal of Applied Physics. It features the AIP logo and the text 'Journal of Applied Physics' at the top. Below this, it says 'Meet The New Deputy Editors'. Three circular portraits of the new deputy editors are shown: Christian Brosseau, Laurie McNeil, and Simon Phillpot, each with their name written below their portrait.

AIP | Journal of Applied Physics

Meet The New Deputy Editors

 Christian Brosseau

 Laurie McNeil

 Simon Phillpot

Magneto-resistive system with concentric ferromagnetic asymmetric nanorings

J. I. Avila,^{a)} M. A. Tumelero, A. A. Pasa, and A. D. C. Viegas

Laboratório de Filmes Finos e Superfícies (LFFS), Departamento de Física, Universidade Federal de Santa Catarina, CP 476 Florianópolis, Brazil

(Received 21 November 2014; accepted 26 February 2015; published online 9 March 2015)

A structure consisting of two concentric asymmetric nanorings, each displaying vortex remanent states, is studied with micromagnetic calculations. By orienting in suitable directions, both the asymmetry of the rings and a uniform magnetic field, the vortices chiralities can be switched from parallel to antiparallel, obtaining in this way the analogue of the ferromagnetic and antiferromagnetic configurations found in bar magnets pairs. Conditions on the thickness of single rings to obtain vortex states, as well as formulas for their remanent magnetization are given. The concentric ring structure enables the creation of magneto-resistive systems comprising the qualities of magnetic nanorings, such as low stray fields and high stability. A possible application is as contacts in spin injection in semiconductors, and estimations obtained here of magneto-resistance change for a cylindrical spin injection based device show significant variations comparable to linear geometries. © 2015 AIP Publishing LLC. [<http://dx.doi.org/10.1063/1.4914346>]

I. INTRODUCTION

Magnetic rings have been considered as memory systems, promising high density and stability.^{1–7} In perfectly symmetric magnetic rings, at zero external field, there appear two characteristic states, one with a head-to-head and a tail-to-tail domain wall, the “onion state” or “O,” and another unique circular domain called the “vortex state” or “V.” Trying to attain any of those states by applying uniform external magnetic fields does not lead to deterministic results.¹ Other possible configuration is the “twisted” state that consists of a “V” state containing a 360° domain wall.⁶ In asymmetric rings, however, it has been experimentally found that the “V” state dominates at zero external field, this depending on the dimensions of the ring and the direction of the field.^{8–11} Moreover, the chirality of the vortex can be manipulated by changing the external field direction. The above properties have been confirmed by direct measurements with several experimental techniques.^{1,10–12}

In electrical spin injection in semiconductors, ferromagnetic electrodes are used to create and detect spin polarized currents in a semiconductor channel.¹³ Unlike spin valves and magnetic tunnel junctions, which use multi-layered systems and currents perpendicular to the planes, spin injection devices are usually fabricated in lateral geometries like the Datta-Das spin transistor.¹⁴ Spin injection, transport, and detection in GaAs and Si have been demonstrated by several approaches, including optical, local, and non-local transport measurements, and the hot-electron method.^{13,15–18} The ferromagnetic electrodes used in transport measurements are rectangular shaped thin film magnets, i.e., bar magnets. Bar magnets have high stray magnetic fields at the ends along their easy axis of the order of the saturation magnetization,¹⁹ so contacts must have dimensions of several micrometers to

reduce the influence of the stray fields on measurements. Magnetic nanorings have low or ideally no stray fields, in the case of perfectly symmetric rings, and portray robust magnetic states that make them well suited as contacts for spintronics devices. It is, however, necessary for the development of a procedure to achieve the equivalent of the ferromagnetic and anti-ferromagnetic configurations of bar contact pairs, and this is given below along with estimations of the magneto-resistance of a spin injection based device.

II. NUMERICAL CALCULATIONS

A diagram of a ring is shown in the inset of Fig. 1, displaying the dimensions: the external circumference radius

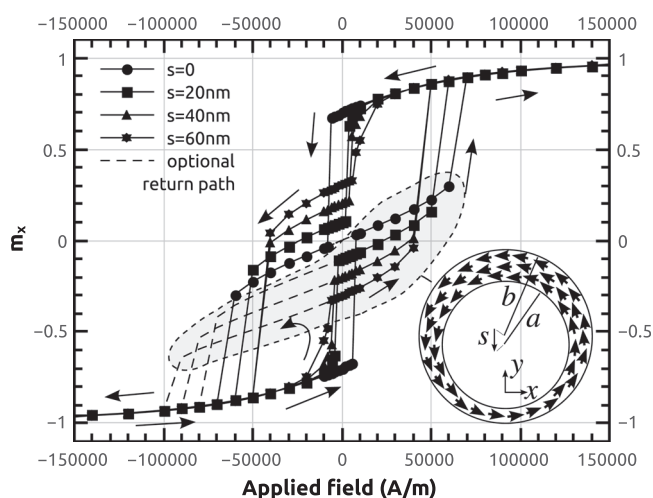


FIG. 1. Hysteresis curves for rings of $t=15$ nm, radii $b=400$ nm, and $a=300$ nm at different shifts s of inner circumference. The optional return paths are obtained by inverting the external field once the “V” state is attained. In the enclosed area, the rings are in anti-clockwise vortex states. As the applied field goes to $\pm 10^6$ A/m, m_x approaches ± 1 (not shown in figure).

^{a)}javila@ulg.ac.be; Current address: Département de Physique, Université de Liège, 4000 Sart Tilman, Belgium.

b and the internal radius a . The vector difference between the center of the inner and outer circumferences s was oriented along the $-y$ axis for all calculations of *individual* rings. The magnetic parameters of permalloy were used, namely, saturation magnetization $M_s = 8.5 \times 10^5$ A/m, and exchange coupling $A = 1.3 \times 10^{-11}$ J/m. Equilibrium magnetic configurations were obtained by solving the Landau-Lifshitz-Gilbert equation with the Nmag 2.0.1 software package.^{20,21} The meshes were obtained with a three dimensional tetrahedral mesher, considering a maximum mesh size of 5 nm. The calculations were made in order to find appropriate rings dimension for the existence of remanent “V” states, and to obtain the hysteresis loops, for magnetic fields ranging from -10^6 A/m up to 10^6 A/m applied in the x direction.

The sizes of the rings considered for the calculations were the following: for rings with fixed $b=200$ nm, inner radii $a = 50, 100, \text{ and } 150$ nm, and thickness values $t = 5, 10, 15, \text{ and } 20$ nm were used. Rings with $b=600$ nm and $a = 450$ nm, $b = 400$ nm and $a = 300$ nm, and $b = 100$ nm and $a = 75$ nm, and thickness $t = 10$ nm and 15 nm were also considered. The value of s was in all cases $0, b/200, 2b/200, \text{ and } 3b/200$.

III. VORTEX STATES

Only rings with 15 nm and 20 nm thicknesses showed remanent vortex states, independent of their radii. To understand this thickness dependence, some insight into the different magnetic configurations exhibited by the rings is needed. At high external field, the magnetization aligns with the field and the average relative magnetization is close to 1 (see Fig. 1). As the external field is reduced, two domain walls (head-to-head and tail-to-tail) appear on opposite sides of the ring, and stabilize at different positions depending on the external field magnitude. When the external field is close to zero, for very thinner rings, the domain walls form a stable 360° wall, the analogue of the “twisted” state.⁶ For thicker rings, however, the walls collapse and the “V” state appears. The “V” state continuously changes its shape under the influence of increasing external fields, until two domain walls appear again.

The formation of the vortex state requires that the head-to-head and tail-to-tail domain walls annihilate each other. This annihilation is only possible if a *vortex wall* is formed during the process, as it is discussed elsewhere²³ based on a topological defects analysis, but the formation of this vortex wall is forbidden energetically in thin and narrow ferromagnets.^{22,23} Therefore, for a defined range of rings width, a threshold ring thickness is expected for vortex states. For the permalloy rings studied in this work, the threshold lies between 10 and 15 nm. Fabrication defects may increase this threshold by creating pinning points for the domain walls, and it may be necessary to experimentally determine it by, for example, patterning ring arrays of different thicknesses and comparing their hysteresis curves with calculations.

The remanence, i.e., the average of magnetization at zero external field, can be used to probe the existence of the “V” state in a ring, since it will have the minimum

remanence compared to any other state. The configuration with the closest value, the “twisted” state, has a remanence of magnitude of several percentage higher, as it can be seen from the numerical results shown in Fig. 2. The remanence in the “V” state can be calculated numerically, but can also be estimated on a geometrical basis. Assuming that the magnetization \mathbf{m} is approximately parallel to the borders of the ring and to its median circumference, it can be derived for $s \ll a$

$$\mathbf{m} \approx \hat{\theta} + \frac{s}{b-a} \cos \theta \hat{r} - \frac{s(a+b)}{2r(b-a)} \cos \theta \hat{r} \quad (1)$$

for anticlockwise sense, where \hat{r} and $\hat{\theta}$ are the unitary cylindrical vectors at an angle θ and a radius r of a coordinate system centered at $-\mathbf{s}\hat{y}/2$. By averaging (1) in the volume of the ring, the x component of the remanent magnetization is calculated to be

$$m_x \approx -\frac{s}{2(b-a)}. \quad (2)$$

Fig. 2 shows plotted results obtained with Eq. (2) vs the corresponding values of m_x obtained from numerical hysteresis curves. A value of ~ 0.99 for the slope of the fitted curve indicates good agreement, suggesting the magnetization of Eq. (1) is a good model for the vortex state and that the simple equation (2) is a fair estimative of the remanence value.

IV. CONCENTRIC ASYMMETRIC RINGS

Two different structures of concentric asymmetric rings were studied by micromagnetic calculations. Figs. 3(a) and 3(b) show the first system, where the displacements s were oriented in opposite directions. At high external field (Fig. 3(a)), the magnetizations of both rings are saturated. When the external field is removed, vortex states are obtained, and the chiralities are found to be antiparallel (see Fig. 3(b)). This system displays the equivalent of an antiferro

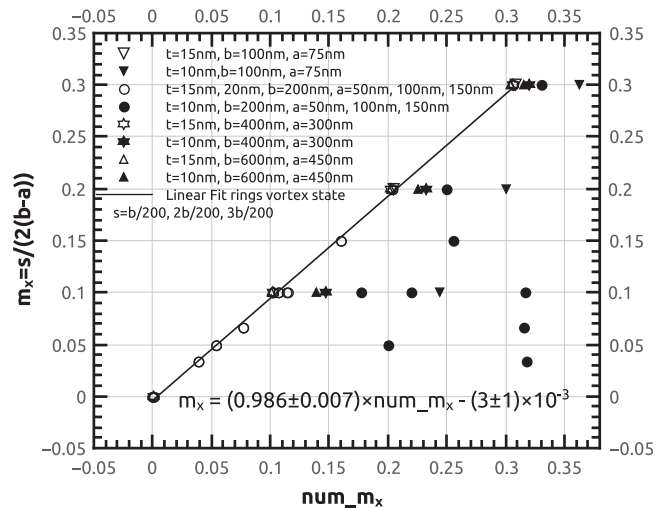


FIG. 2. Comparison of values of m_x obtained from Eq. (2) for remanent magnetization at zero external field vs numerical results $\text{num_}m_x$, in absolute value. Unfilled symbols correspond to rings in the vortex state, and filled symbols to rings in the “twisted” state.

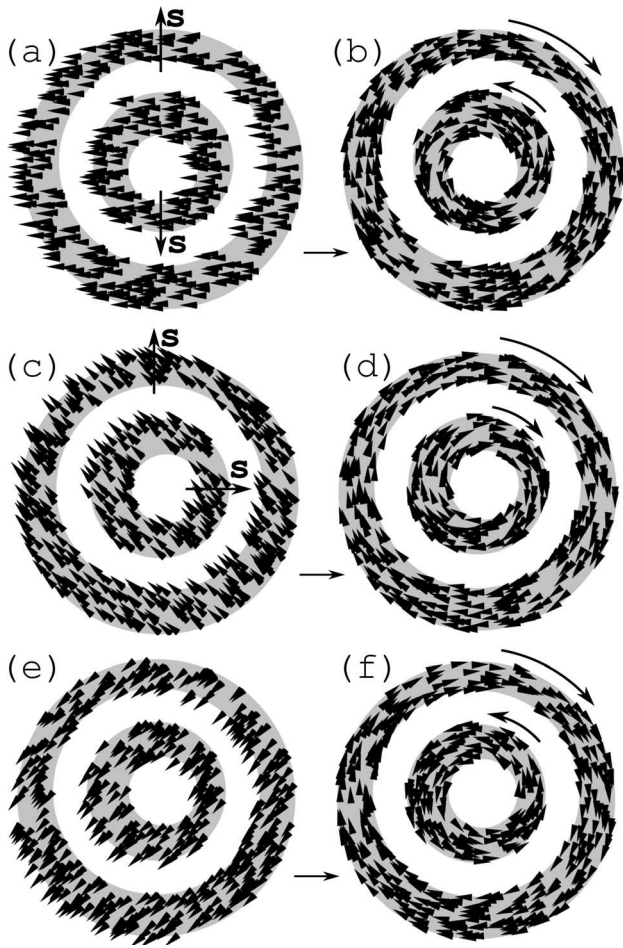


FIG. 3. (a) and (b): System of two asymmetrical rings with dimensions $t = 15$ nm, $b = 400$ nm, $a = 300$ nm, $s = 20$ nm \hat{y} and $b = 200$ nm, $a = 100$ nm, $s = -20$ nm \hat{y} . (a) Both rings are saturated in the $-\hat{x}$ direction by the effect of a field of 10^6 A/m. (b) After the external field is removed, the rings are in the “V” state with opposed rotation sense. (c)–(f) System with parameters $t = 15$ nm, $b = 400$ nm, $a = 300$ nm, $s = 20$ nm \hat{y} and $b = 200$ nm, $a = 100$ nm, $s = 20$ nm \hat{x} . (c) Field of 10^6 A/m applied in $(-\hat{x} + \hat{y})$ direction (d) No external field. (e) Field of 10^6 A/m applied along $-(\hat{x} + \hat{y})$. (f) No external field.

configuration between the rings at zero external field, but it requires the permanent application of a high external field to have parallel magnetization (Fig. 3(a)).

It must be noticed that it is not necessary to apply the external field perpendicular to the asymmetry axis of the ring, to get the “V” state, a fact that was already reported¹¹ for individual rings. That is because the chirality of the remanent magnetization is determined by the magnetization component perpendicular to s of the wider part of the ring at saturation.

Taking advantage of this fact, a second system of concentric rings shown in Figs. 3(c)–3(f) was considered. The displacements s were now oriented in perpendicular directions. For the smaller ring, it was chosen $s = s\hat{x}$, and $s = s\hat{y}$ for the larger one. By first saturating along the $-\hat{x} + \hat{y}$ direction (Fig. 3(c)) and then removing the external field, the chiralities are found to be parallel (Fig. 3(d)). Alternatively, by saturating in the $-(\hat{x} + \hat{y})$ direction (Fig. 3(e)), the chiralities are found to be antiparallel when the external field is set to zero (Fig. 3(f)).

Then, parallel and antiparallel remanent chiralities can be obtained in the rings by changing the saturation field direction, obtaining the equivalent of ferro and antiferro configurations of bar magnets. This represents a radically different approach to current geometries, where parallel or antiparallel magnetic configurations are set by exploiting the magnets coercive field dependence on width or by the use of pinning layers. In this particular system of Figs. 3(c)–3(f), the stray fields between the rings were found to be of the order of 10^3 A/m, a low value compared to the saturation magnetization of permalloy.

V. SPIN INJECTION WITH CYLINDRICAL CONTACTS

By patterning asymmetric concentric ferromagnetic nanoring electrodes with a tunneling barrier on a semiconductor substrate, with suitable barrier, interface, and spin resistances,¹⁴ stable states of parallel and antiparallel magnetization chiralities can be set for spin injection and detection. The spatial dependence of the spin will have, however, some differences compared to linear geometries. The spin density S of an ensemble of spins in a purely diffusive regime and without magnetic fields is determined by the special case of the Bloch-Torrey equations^{24,27}

$$\frac{\partial S}{\partial t} = D_s \left(\nabla^2 S - \frac{S}{L^2} \right), \quad (3)$$

where L is the spin diffusion length and D_s the diffusion constant. In the linear one-dimensional case, S will fall as $e^{-|x|/L}$ away from a source at $x=0$. In a steady state two-dimensional system with axial symmetry, Eq. (3) reduces to the modified Bessel equation in the radial coordinate. For spin injection by a ring source in the vortex state, solutions of the form $S = S(r)\hat{\theta}$ are looked for. Then it is found that S varies as $I_1(r/L)$ inside the zone limited by the ring and as $K_1(r/L)$ out of it, where I_1 and K_1 are modified Bessel functions of the first and the second kind, respectively. For $r \ll L$, the function $I_1(r/L) \sim r/2L$ and K_1 diverges as L/r , and for $r \gg L$, $I_1(r/L) \sim \sqrt{\frac{L}{2\pi r}} e^{r/L}$ and $K_1(r/L) \sim \sqrt{\frac{\pi L}{2r}} e^{-r/L}$.²⁵

Considering a 1-D channel for spin along a direction \hat{r} , with possible $\pm\hat{\theta}$ spin directions, the spin accumulation $\Delta\mu = \mu_+ - \mu_-$ is proportional to $S(r)$, as $\Delta\mu$ is proportional to the modulus of the electronic out of equilibrium magnetization that is also proportional to S .^{26,27} The functions I_1 and K_1 consider the metrics and the overlap of spin coming from opposite sides of the ring. They are valid for the surface of the semiconductor substrate in the space between the rings in a 3D real system.

The Valet and Fert approach^{14,26} was used to estimate the resistance change between parallel and antiparallel chiralities in a concentric ring system. A model of three contiguous regions (I), (II), and (III) was considered. In the outer regions (I) and (III), corresponding to the ferromagnetic contacts, the linear solutions were used, and only in the central region (II), where the semiconductor material lies, the axially symmetric solution was used

$$(I) \text{ for } x \text{ in } [\bar{r}_0, \bar{r}_1],$$

$$\Delta\mu_I = Ae^{(x-\bar{r}_1)/L_F}, \quad \bar{r}_1 - \bar{r}_0 \gg L_F, \quad (4)$$

$$(II) \text{ for } x \text{ in } [\bar{r}_1, \bar{r}_2],$$

$$\Delta\mu_{II} = BI_1[x/L_N] + CK_1[x/L_N], \quad (5)$$

$$(III) \text{ for } x \text{ in } [\bar{r}_2, \bar{r}_3],$$

$$\Delta\mu_{III} = De^{-(x-\bar{r}_2)/L_F}, \quad \bar{r}_3 - \bar{r}_2 \gg L_F, \quad (6)$$

with L_N and L_F as the spin diffusion length in the semiconductor and ferromagnetic materials, respectively, and A , B , C , and D as constants that must be determined. Using spin dependant interface resistances $r_{+(-)} = 2r_b(1 - (+)\gamma)$, spin dependant resistivity in the ferromagnetic material $\rho_{\uparrow(\downarrow)} = 2(1 - (+)\beta)\rho_F$ and in the semiconductor $\rho_{\uparrow(\downarrow)} = 2\rho_N$, and imposing boundary conditions on the chemical potentials μ_{\pm} and currents J_{\pm} ^{14,26} described in the Appendix, it is found that the resistance change is given by

$$\Delta R = 2r_N L_N (\bar{r}_1 + \bar{r}_2) (\beta r_F + \gamma r_b)^2 / (Q + P), \quad (7)$$

with

$$Q = \left[kI_0 \left[\frac{\bar{r}_2}{L_N} \right] - II_1 \left[\frac{\bar{r}_2}{L_N} \right] \right] \left[mK_0 \left[\frac{\bar{r}_1}{L_N} \right] + nK_1 \left[\frac{\bar{r}_1}{L_N} \right] \right], \quad (8)$$

$$P = \left[-mI_0 \left[\frac{\bar{r}_1}{L_N} \right] + nI_1 \left[\frac{\bar{r}_1}{L_N} \right] \right] \left[kK_0 \left[\frac{\bar{r}_2}{L_N} \right] + lK_1 \left[\frac{\bar{r}_2}{L_N} \right] \right], \quad (9)$$

$$k = \bar{r}_2(r_b + r_F), \quad (10)$$

$$l = L_N(r_b + r_F) - \bar{r}_2 r_N, \quad (11)$$

$$m = \bar{r}_1(r_b + r_F), \quad (12)$$

$$n = L_N(r_b + r_F) + \bar{r}_1 r_N, \quad (13)$$

$$r_F = \rho_F L_F, \quad (14)$$

$$r_N = \rho_F L_N. \quad (15)$$

As discussed elsewhere,¹⁴ this expression must be compared to a periodic structure in a ferromagnetic or parallel configuration with resistance R^P . The details for the calculation of R^P are given in the Appendix.

In Fig. 4, the ratio $\Delta R/R^P$ is plotted as a function of the interface resistance r_b for cobalt parameters used in similar calculations,¹⁴ with L_N taken from Ref. 13, and listed in Fig. 4. For those parameters, it is seen that the resistance difference has a significant maximum in a window of about two orders of magnitude of interface resistance centred at the maximum, approaching $\Delta R/R^P$ ratios calculated for parallel 1-D geometries (see Fig. 3 in the work of Fert and Jaffrès¹⁴). In the same figure, the ratio $\Delta R/R^P$ is plotted for a lower $r_F = 2.9 \times 10^{-16} \Omega\text{m}^2$ closer to permalloy, calculated using a resistivity of $5.8 \times 10^{-8} \Omega\text{m}$ and $L_F = 5 \text{ nm}$,²⁸ and a $r_N = 3 \times 10^{-11} \Omega\text{m}^2$ obtained using the same $L_N = 600 \text{ nm}$ but a different resistivity of $5 \times 10^{-5} \Omega\text{m}$ for highly doped silicon, in order to guarantee a narrow depletion region.¹³ The value of r_F has little influence on the position of the peaks of the curves that seem to be close to r_N . Optimum resistance area ratios r_b for a given geometry can be determined from the

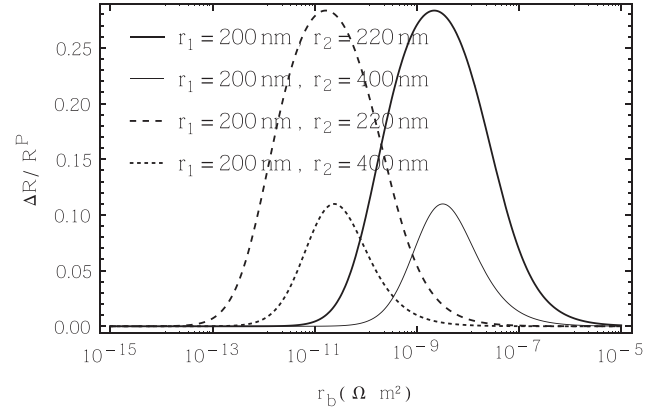


FIG. 4. Relative resistance variation vs interface resistance. Parameters used for continuous line curves are $r_F = 4.5 \times 10^{-15} \Omega\text{m}^2$ (Cobalt), $r_N = 4 \times 10^{-9} \Omega\text{m}^2$, $L_N = 600 \text{ nm}$, $L_F = 60 \text{ nm}$, $t_F = L_F$, $\beta = 0.46$, $\gamma = 0.5$, and for dashed curves $r_F = 2.9 \times 10^{-16} \Omega\text{m}^2$ (Permalloy), $r_N = 3 \times 10^{-11} \Omega\text{m}^2$ (highly doped silicon), $L_F = 5 \text{ nm}$, same L_N , β , and γ .

formulas derived here for ΔR and R^P to choose the appropriate tunnel barrier that for the last parameters corresponds to $r_b \approx 1.6 \times 10^{-11} \Omega\text{m}^2$. Then the concentric nanorings structure represents a viable geometry for spin injection devices.

VI. CONCLUSION

For the permalloy parameters used here, it is found by numerically solving the LLG equation that the vortex state readily forms for nanorings of thickness equal or greater than 15 nm. An analytic expression is given for the magnetization of the rings in the vortex states, and by averaging it, a formula is obtained for the remanence that can serve to test the presence of the state through hysteresis curve measurements. Vortex states are also found to be possible in concentric asymmetric rings, and a geometry, where their chiralities can be switched from parallel to antiparallel by uniform external fields is proposed for spin injection experiments in semiconductors. Expressions for the resistance variations between parallel and antiparallel chiralities are found, and significant values comparable to linear systems can be obtained by using suitable interface resistances.

ACKNOWLEDGMENTS

The authors wish to thank Brazilian Projects CAPES/PNPD 2585/2011, CNPq 478047/2012-6, and agencies CNPq, FINEP, and FAPESC for the financial support. The authors also thank Hans Fangohr for his help with the nmag package.

APPENDIX: MAGNETORESISTANCE CALCULATION

The following equations describe the chemical potentials and currents in the three regions for the parallel configuration:

$$\mu_{I\pm}[x] = Jze\rho_F(1 - \beta^2) \pm \frac{A}{2}(1 \mp \beta)e^{(x-\bar{r}_1)/L_F}, \quad (A1)$$

$$J_{I\pm}[x] = \frac{J}{2}(1 \pm \beta) \pm \frac{A}{4e r_F} e^{(x-\bar{r}_1)/L_F}, \quad (A2)$$

$$\mu_{II\pm}[x] = Jze\rho_N + K_{II}\pm \frac{1}{2}(BI_1(x/L_N) + CK_1(x/L_N)), \quad (\text{A3})$$

$$J_{II\pm}[x] = \frac{J}{2}\pm \frac{1}{4e r_N}(BI'_1(x/L_N) + CK'_1(x/L_N)), \quad (\text{A4})$$

$$\mu_{III\pm}[x] = Jze\rho_F(1 - \beta^2) + K_{III}\pm \frac{D}{2}(1\mp\beta)e^{-(x-\bar{r}_2)/L_F}, \quad (\text{A5})$$

$$J_{III\pm}[x] = \frac{J}{2}(1\pm\beta)\mp \frac{D}{4e r_F}e^{-(x-\bar{r}_2)/L_F}, \quad (\text{A6})$$

where e is the electron charge and $J = J_+ + J_-$ is the total current. The boundary conditions are

$$\mu_{II\pm}[\bar{r}_1] - \mu_{I\pm}[\bar{r}_1] = e r_{\pm} J_{I\pm}[\bar{r}_1], \quad (\text{A7})$$

$$\mu_{III\pm}[\bar{r}_2] - \mu_{II\pm}[\bar{r}_2] = e r_{\pm} J_{III\pm}[\bar{r}_2], \quad (\text{A8})$$

$$J_{I+}[\bar{r}_1] = J_{II+}[\bar{r}_1], \quad (\text{A9})$$

$$J_{II+}[\bar{r}_2] = J_{III+}[\bar{r}_2]. \quad (\text{A10})$$

Solving for the unknown constants, the resistance is then calculated by

$$R^{pa} = \frac{1}{2eJ} [\mu_{III+}[\bar{r}_3] + \mu_{III-}[\bar{r}_3] - \mu_{I+}[\bar{r}_0] - \mu_{I-}[\bar{r}_0]]. \quad (\text{A11})$$

For the anti-ferromagnetic configuration, the indexes in region (III) and the boundary resistance at \bar{r}_2 are exchanged, i.e., $\pm \rightarrow \mp$. The resistance R^a is then calculated by the same formula for R^{pa} is given in (A11). Equation (7) is obtained by calculating $\Delta R = R^a - R^{pa}$. A fictitious system is used to calculate the periodic resistance R^P . Again, solutions for a linear system are used in the outer regions and axially symmetric solutions in the central region

(I) for x in $[\bar{r}_1 - t_F/2, \bar{r}_1]$,

$$\Delta\mu_I = A \cosh[(x - (\bar{r}_1 - t_F/2))/L_F] + B \sinh[(x - (\bar{r}_1 - t_F/2))/L_F], \quad (\text{A12})$$

(II) for x in $[\bar{r}_1, \bar{r}_2]$,

$$\Delta\mu_{II} = CI_1(x/L_N) + DK_1(x/L_N), \quad (\text{A13})$$

(III) for x in $[\bar{r}_2, \bar{r}_2 + t_F/2]$,

$$\Delta\mu_{III} = E \cosh[(x - (\bar{r}_2 + t_F/2))/L_F] + F \sinh[(x - (\bar{r}_2 + t_F/2))/L_F], \quad (\text{A14})$$

where the inner and outer ferromagnetic contacts have thickness $t_F/2$. Periodic conditions are established between the outer surfaces, namely, $J_{I\pm}[\bar{r}_1 - t_F/2] = J_{III\pm}[\bar{r}_2 + t_F/2]$ and $\Delta\mu_{I\pm}[\bar{r}_1 - t_F/2] = \Delta\mu_{III\pm}[\bar{r}_2 + t_F/2]$, giving $A = E$ and $B = F$. The resistance R^P can be obtained then by the same procedure used to get R^{pa} . The result is

$$R^P = a_1 + \frac{a_2}{a_3} + \frac{a_4}{a_3(a_5 + a_6)}, \quad (\text{A15})$$

with

$$a_1 = 2(1 - \gamma)r_b + \rho_N(\bar{r}_2 - \bar{r}_1) - 2(1 - \beta)\beta r_F \tanh\left[\frac{t_F}{2L_F}\right], \quad (\text{A16})$$

$$a_2 = 2r_{c2} \left[r_N (\Delta K_1 \Delta I'_1 - \Delta I_1 \Delta K'_1) + 2 \left((1 - \gamma)r_b + (1 - \beta)r_F \tanh\left[\frac{t_F}{2L_F}\right] \right) \times \left(\Delta I'_1 K'_1 \left[\frac{\bar{r}_1}{L_N}\right] - \Delta K'_1 I'_1 \left[\frac{\bar{r}_1}{L_N}\right] \right) \right], \quad (\text{A17})$$

$$a_3 = r_N \cosh\left[\frac{t_F}{2L_F}\right] (\Delta K_1 \Delta I'_1 - \Delta I_1 \Delta K'_1) + 2r_{c1} \left(\Delta I'_1 K'_1 \left[\frac{\bar{r}_1}{L_N}\right] - \Delta K'_1 I'_1 \left[\frac{\bar{r}_1}{L_N}\right] \right), \quad (\text{A18})$$

$$a_4 = 2 \sinh\left[\frac{t_F}{2L_F}\right] r_{c2}^2 r_N^2 (\Sigma K_1 \Delta I'_1 - \Sigma I_1 \Delta K'_1) \times (\Delta K_1 \Sigma I'_1 - \Delta I_1 \Sigma K'_1) \quad (\text{A19})$$

$$a_5 = 2 \sinh\left[\frac{t_F}{2L_F}\right] r_N \left(I_1 \left[\frac{\bar{r}_1}{L_N}\right] \left(\cosh\left[\frac{t_F}{2L_F}\right] r_N \Delta K_1 + r_{c1} \Delta K'_1 \right) - K_1 \left[\frac{\bar{r}_1}{L_N}\right] \left(\cosh\left[\frac{t_F}{2L_F}\right] r_N \Delta I_1 + r_{c1} \Delta I'_1 \right) \right) + r_N r_F (\Delta K_1 \Delta I'_1 - \Delta I_1 \Delta K'_1), \quad (\text{A20})$$

$$a_6 = 2 \sinh\left[\frac{t_F}{2L_F}\right] r_{c1} r_N \left(\Sigma I_1 K'_1 \left[\frac{\bar{r}_1}{L_N}\right] - \Sigma K_1 I'_1 \left[\frac{\bar{r}_1}{L_N}\right] \right) + 2r_{c1} r_{c3} \left(\Delta I'_1 K'_1 \left[\frac{\bar{r}_1}{L_N}\right] - \Delta K'_1 I'_1 \left[\frac{\bar{r}_1}{L_N}\right] \right) \quad (\text{A21})$$

and with

$$I'_1[z] = \frac{1}{2} [I_0(z) + I_2(z)], \quad (\text{A22})$$

$$K'_1[z] = -\frac{1}{2} [K_0(z) + K_2(z)], \quad (\text{A23})$$

$$\Delta I_1 = I_1 \left[\frac{\bar{r}_2}{L_N}\right] - I_1 \left[\frac{\bar{r}_1}{L_N}\right], \quad (\text{A24})$$

$$\Delta K_1 = K_1 \left[\frac{\bar{r}_2}{L_N}\right] - K_1 \left[\frac{\bar{r}_1}{L_N}\right], \quad (\text{A25})$$

$$\Sigma I_1 = I_1 \left[\frac{\bar{r}_2}{L_N}\right] + I_1 \left[\frac{\bar{r}_1}{L_N}\right], \quad (\text{A26})$$

$$\Sigma K_1 = K_1 \left[\frac{\bar{r}_2}{L_N}\right] + K_1 \left[\frac{\bar{r}_1}{L_N}\right], \quad (\text{A27})$$

$$\Delta I'_1 = I'_1 \left[\frac{\bar{r}_2}{L_N}\right] - I'_1 \left[\frac{\bar{r}_1}{L_N}\right], \quad (\text{A28})$$

$$\Delta K'_1 = K'_1 \left[\frac{\bar{r}_2}{L_N}\right] - K'_1 \left[\frac{\bar{r}_1}{L_N}\right], \quad (\text{A29})$$

$$\Sigma I'_1 = I'_1 \left[\frac{\bar{r}_2}{L_N}\right] + I'_1 \left[\frac{\bar{r}_1}{L_N}\right], \quad (\text{A30})$$

$$\Sigma K'_1 = K'_1 \left[\frac{\bar{r}_2}{L_N}\right] + K'_1 \left[\frac{\bar{r}_1}{L_N}\right], \quad (\text{A31})$$

$$r_{c1} = r_b \cosh[t_F/(2L_F)] + r_F \sinh[t_F/(2L_F)], \quad (\text{A32})$$

$$r_{c2} = \gamma r_b \cosh[t_F/(2L_F)] + \beta r_F \sinh[t_F/(2L_F)], \quad (\text{A33})$$

$$r_{c3} = r_F \cosh[t_F/(2L_F)] + r_b \sinh[t_F/(2L_F)]. \quad (\text{A34})$$

- ¹M. Kläui, C. A. F. Vaz, L. Lopez-Diaz, and J. A. C. Bland, *J. Phys.: Condens. Matter* **15**, R985–R1023 (2003).
- ²D. K. Singh, R. Krotkov, and M. T. Tuominen, *Phys. Rev. B* **79**, 184409 (2009).
- ³Gabriel D. Chaves-O'Flynn, A. D. Kent, and D. L. Stein, *Phys. Rev. B* **79**, 184421 (2009).
- ⁴J.-G. Zhu, Y. Zheng, and G. A. Prinz, *J. Appl. Phys.* **87**, 6668 (2000).
- ⁵H. X. Wei, F. Q. Zhu, X. F. Han, Z. C. Wen, and C. L. Chien, *Phys. Rev. B* **77**, 224432 (2008).
- ⁶F. J. Castano, C. A. Ross, A. Eilez, W. Jung, and C. Frandsen, *Phys. Rev. B* **69**, 144421 (2004).
- ⁷T. Yang, N. R. Pradhan, A. Goldman, A. S. Licht, Y. Li, M. Kemei, M. T. Tuominen, and K. E. Aidala, *Appl. Phys. Lett.* **98**, 242505 (2011).
- ⁸E. Saitoh, M. Kawabata, K. Harii, and H. Miyajim, *J. Appl. Phys.* **95**, 1986 (2004).
- ⁹D. K. Singh, T. Yang, and M. T. Tuominen, *Phys. B: Cond. Matter* **405**, 4377–4381 (2010).
- ¹⁰F. Giesen, J. Podbielski, B. Botters, and D. Grundler, *Phys. Rev. B* **75**, 184428 (2007).
- ¹¹F. Q. Zhu, G. W. Chern, O. Tchernyshyov, X. C. Zhu, J. G. Zhu, and C. L. Chien, *Phys. Rev. Lett.* **96**, 027205 (2006).
- ¹²C. A. F. Vaz, T. J. Hayward, J. Llandro, F. Schackert, D. Morecroft, J. A. C. Bland, M. Klui, M. Laufenberg, D. Backes, U. Rdiger, F. J. Castao, C. A. Ross, L. J. Heyderman, F. Nolting, A. Locatelli, G. Faini, S. Cherifi, and W. Wernsdorfer, *J. Phys.: Condens. Matter* **19**, 255207 (2007).
- ¹³Ron Jansen, *Nat. Mater.* **11**, 400–408 (2012).
- ¹⁴A. Fert and H. Jaffrès, *Phys. Rev. B* **64**, 184420 (2001).
- ¹⁵C. L. Dennis, J. F. Gregg, G. J. Ensell, and S. M. Thompson, *J. Appl. Phys.* **100**, 043717 (2006).
- ¹⁶T. Appelbaum, B. Huang, and D. J. Monsma, *Nature* **447**, 295–298 (2007).
- ¹⁷C. I. L. de Araujo, M. A. Tumelero, J. I. Avila, A. D. C. Viegas, N. Garcia, and A. A. Pasa, *J. Supercond. Novel Mag.* **26**, 3449–3454 (2013).
- ¹⁸O. M. J. van't Erve, A. T. Hanbicki, M. Holub, C. H. Li, C. Awo-Affouda, P. E. Thompson, and B. T. Jonker, *Appl. Phys. Lett.* **91**, 212109 (2007).
- ¹⁹F. G. Monzon, D. S. Patterson, and M. L. Roukes, *J. Magn. Magn. Mater.* **195**, 19–25 (1999).
- ²⁰T. Fischbacher, M. Franchin, G. Bordignon, and H. Fangohr, *IEEE Trans. Magn.* **43**, 6, 2896–2898 (2007).
- ²¹T. Fischbacher, M. Franchin, G. Bordignon, A. Knittel, and H. Fangohr, *J. Appl. Phys.* **105**, 07D527 (2009).
- ²²R. D. McMichael and M. J. Donahue, *IEEE Trans. Magn.* **33**, 5, 4167–4169 (1997).
- ²³O. Tchernyshyov and G.-W. Chern, *Phys. Rev. Lett.* **95**, 197204 (2005).
- ²⁴J. Fabian, A. Matos-Abiague, C. Ertler, P. Stano, and I. Žutić, *Acta Phys. Slov.* **57**, 565 (2007).
- ²⁵I. S. Gradshteyn and I. M. Ryzhik, *Table of Integrals, Series and Products*, 7th ed. (Elsevier/Academic Press, Amsterdam, 2007).
- ²⁶T. Valet and A. Fert, *Phys. Rev. B* **48**, 7099 (1993).
- ²⁷I. Žutić, J. Fabian, and S. Das Sarma, *Rev. Mod. Phys.* **76**, 323 (2004).
- ²⁸S. Dubois, L. Piraux, J. M. George, K. Ounadjela, J. L. Duvail, and A. Fert, *Phys. Rev. B* **60**, 477 (1999).